I. ARRAY OF DOUBLE-WELL POTENTIALS

The trapping potential is the sum of three optical lattices realized with the three laser beams at $\lambda_1 \simeq 1013$nm, $\lambda_2 \simeq 1064$ nm and $\lambda_3 \simeq 1120$nm retro-reflected on a mirror placed at ~ 25 cm from the atoms

$$V(x) = \sum_{i=1,2,3} V_i \sin^2(k_i x + \phi_i) \tag{SI.1}$$

where $k_i = 2\pi/\lambda_i$, V_i and ϕ_i are the depth and the phase of $i-$th lattice. Following the analysis reported in [1], we can demonstrate that in the low depth regime, i.e. $V_i \ll E_{R_i} = \hbar^2 k_i^2/2m$, where m is the mass of the atom, the choice of the wavelengths such that $k_1 - k_2 = k_2 - k_3 = \Delta k$ allows to provide an effective trapping potential

$$V_{\text{eff}}(x) = -\frac{V_1 V_2 \cos(2\Delta k x + 2(\phi_1 - \phi_2))}{16 E_{R_2}} - \frac{V_2 V_3 \cos(2\Delta k x + 2(\phi_2 - \phi_3))}{16 E_{R_2}} - \frac{V_1 V_3 \cos(4\Delta k x + 2(\phi_1 - \phi_3))}{16 E_{R_2}} \tag{SI.2}$$

Please note that the three terms are the result of the beating between the lattices with wavelengths λ_1 and λ_2, λ_2 and λ_3 and λ_1 and λ_3 respectively. The first two lattices have a spatial periodicity of $\simeq 10\mu$m, while the third one of $\simeq 5\mu$m.
In order to achieve an array of balanced double wells, we choose $\phi_1 = \phi_2$ and $\phi_3 = \phi_2 + \pi$ and we get

$$V_{\text{eff}}(x) = -\frac{(V_1 - V_3) V_2 \cos(2\Delta k x)}{16 E_{R_2}} + \frac{V_1 V_3 \cos(4\Delta k x)}{16 E_{R_2}} \tag{SI.3}$$

Interestingly, in this configuration the first two lattices have an opposite phase and, for $V_1 = V_3$, they perfectly cancel each other. During the initial loading of the BECs in the 10 μm BNSL, $V_1 \simeq 400\,$nK and $V_2 \simeq 350\,$nK. The barrier height tunability is provided by the control of V_3 that can achieve a maximum value of $\simeq 250\,$nK.

The three lasers are locked to the same optical cavity using a transfer frequency PDH technique [2–4] that allows to tune the laser frequency plus/minus half the free spectral range of the cavity. The full width at half maximum of the locked lasers is $\simeq 100$kHz. The cavity geometry is a semi-circular one, with one mirror almost plane and the other one with a radius of curvature of $\sim$14 cm. The finesse is ~ 2400 for λ_1, ~ 4500 for λ_2 and ~ 3100 for λ_3. The different finesses are due slightly different reflectivities for the wavelenghts. The phase of the lattices can be changed tuning the frequency of the lasers that are retroreflected on a mirror placed 25 cm away from the atoms. At full barrier height, a frequency shift of 300 kHz of one of the lasers, corresponds to a phase shift of the lattice of 10 mrad and an energy mismatch, common to all the double wells, of 5 Hz between the two modes. A larger frequency shift that breaks the condition $k_1 - k_2 = k_2 - k_3$ introduces an effective harmonic confinement along the lattice direction. Using a numerical simulation we quantify a 10 Hz longitudinal confinement, when the laser frequency of one laser is tuned by 0.01 nm. Depending on the sign of the detuning the potential can be confining or anti-confining.

The BNSLs are generated by two diode lasers and one Nd :YAG laser, injected into three independent solid state amplifiers. The depths of the lattice potentials are adjusted measuring the oscillation frequencies (of the order of 180 Hz) of the condensates around the minima of the effective potentials of the BNSLs formed by the lattice couples λ_1, λ_2 and λ_2, λ_3 and by measuring the tunneling frequency between the two wells.

II. EXTERNAL HARMONIC POTENTIAL

The external potential used to create the differential energy mismatch δ between two neighboring double wells is created by a vertical laser beam with wavelength $\lambda \simeq 1064$ nm. This beam is focused on the atoms with a beam waist of ~ 50 μm, significantly larger than the separation between two distinct double-wells. In Fig. 1 we report a typical trapping frequency measurement.

III. CALIBRATION OF THE EXTERNAL MAGNETIC FIELD

In our experiment the Feshbach magnetic field is generated by a pair of circular coils placed $\sim \pm 2$ cm above and below the atomic sample. The calibration of the magnetic field (B_F) is performed by exciting the magnetically sensitive RF transition from the internal sate $|F = 1, m_F = -1\rangle$ to $|F = 1, m_F = 0\rangle$. The amplitude and duration of the pulsed current is chosen to achieve a 50% probability transfer when the resonance condition is achieved. In Fig. 2 a) we report a typical measurement of the transferred population as a function of the RF current frequency. Using a Gaussian fit, we determine the position of the peak center and from the Breit-Rabi formula [5, 6], we can convert

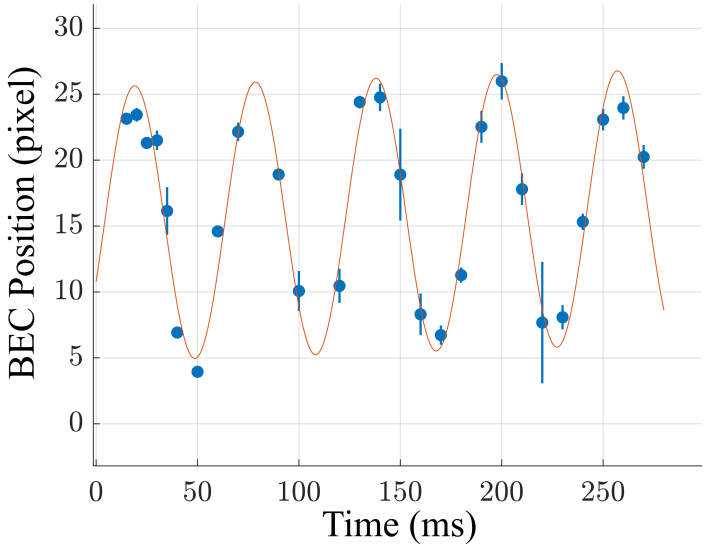

FIGURE 1: **Vertical beam trapping frequency.** Measurement of the BEC position as a function of time. The data are fitted with a sinusoidal function to determine the trapping frequency (for his specific set of measurements $\omega = 2\pi 16.8(1)$ Hz).

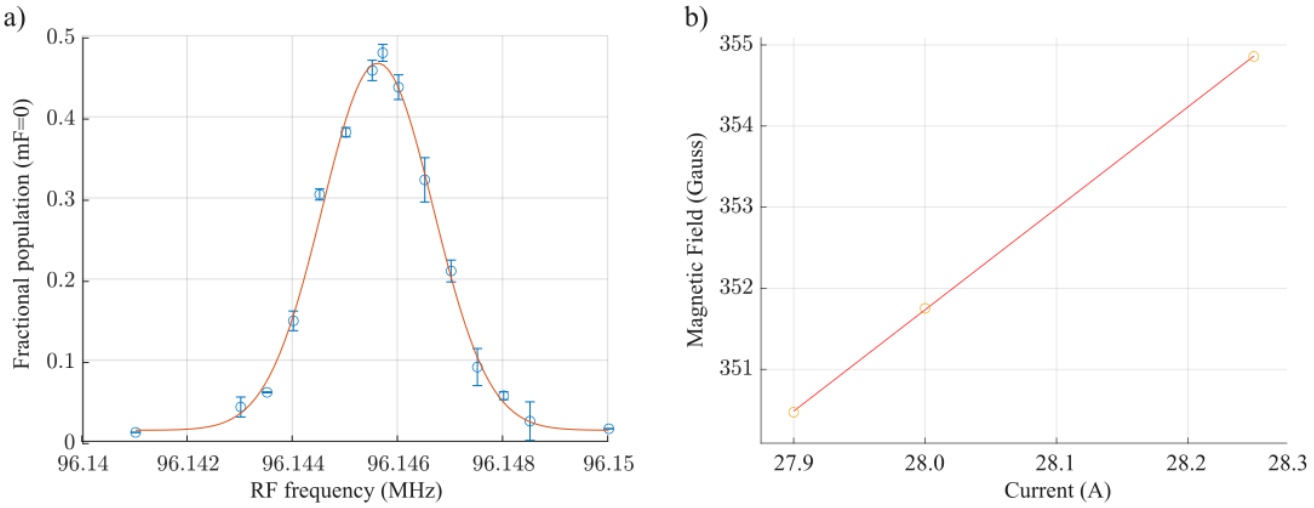

FIGURE 2: **Magnetic Field calibration**. a) Resonance peak of the transition from $|F = 1, mF = -1\rangle$ to $|F = 1, mF = 0\rangle$ as a function of the RF frequency. The data are fitted with a Gaussian function. b)Measured B_F as a function of the current in the Feshbach coils. Solid line is a linear fit to the data.

it from Hz unit to magnetic field unit. We repeat the measurement for different values of the current in the Feshbach coils to achieve the magnetic field vs RF frequency calibration shown in Fig. 2 b).

In addition, we estimate the long term fluctuations of B_F by choosing a magnetic field and a RF pulse to achieve a transferred population of ≈ 0.25 and repeating the measurement several times for a total duration of ~ 2 hours. For small magnetic field variations, the linear dependence of the transferred population on the value of B_F allows to convert the measurement of the atoms in the $|F = 1, m_F = 0\rangle$ to a measurement of the external Feshbach magnetic field. Collection of ~ 150 measurements is reported in the histogram of Fig. 3.

IV. DERIVATION OF EQ. (2) ISE OF BEAM SPLITTERS

In the following, we derive the Eq. (2) reported in the main paper. We model each Mach-Zehnder interferometer as a system of N particles in two bosonic modes, a and b. In the ideal scenario, for non-interacting atoms, the first

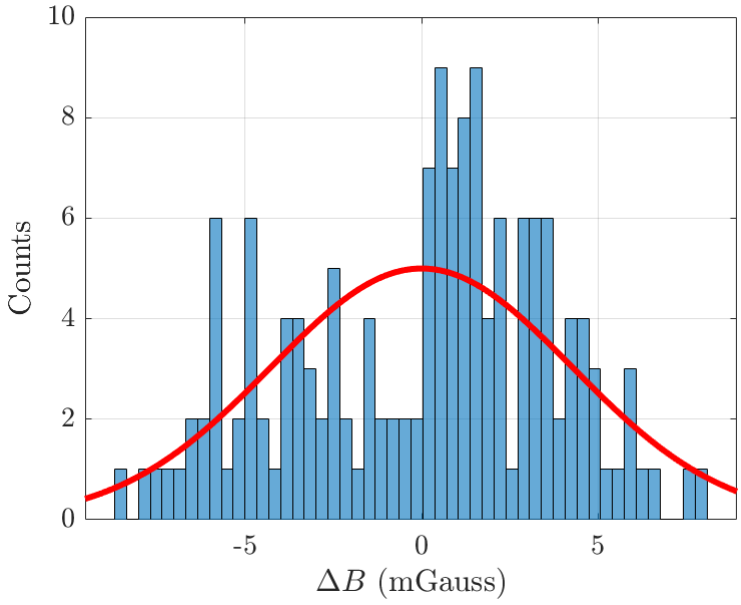

FIGURE 3: **Magnetic Noise**. Histogram of the fluctuations of the measurements of B_F performed over a time interval of ~ 2 hours. The data are fitted with a Gaussian distribution (solid line) with a width of 4.3(12) mGauss.

beam splitter (BS) prepares a binomial distribution of particles among the two modes,

$$|\psi_{\rm BS}\rangle = \sum_{\mu=-N/2}^{N/2} \sqrt{\frac{N!}{(N/2-\mu)!(N/2+\mu)!}} \left(\cos\frac{\theta}{2}\right)^{N/2-\mu} \left(\sin\frac{\theta}{2}\right)^{N/2+\mu} |N/2-\mu\rangle_a \, |N/2+\mu\rangle_b \,, \tag{SI.4}$$

Here $|N/2-\mu\rangle_a$ and $|N/2+\mu\rangle_b$ are Fock states corresponding to $N/2+\mu$ particles in mode a and $N/2+\mu$ particles in mode b. The parameter θ is related to the effective reflectivity ($\langle\psi_{\rm BS}| N_a |\psi_{\rm BS}\rangle = N\cos^2\theta/2$) and transitivity ($\langle\psi_{\rm BS}| N_a |\psi_{\rm BS}\rangle = N\sin^2\theta/2$) of the beam splitter, where N_a and N_b are number of particles operators. Notice that $z=\cos\theta$ and the balanced beam splitter is recovered for $\theta=\pi/2$. We consider the case where $\theta\approx\pi/2$ and $N\gg 1$. We can thus replace the sum in Eq. (SI.4) with an integral extending from $\pm\infty$, and approximate the binomial distribution with the Gaussian

$$|\psi_{\rm BS}\rangle = \int_{-\infty}^{+\infty} d\mu \; \frac{e^{-\frac{(\mu-\mu_0)^2}{4\sigma^2}}}{(2\pi\sigma^2)^{1/4}} \, |\mu\rangle \,, \tag{SI.5}$$

centered in $\mu_0=(N/2)\cos\theta$ and with width $\sigma^2=(N/4)\sin\theta$. Let us introduce the relative number of particles operator $J_z=(N_a-N_b)/2$. During phase encoding (PE), the systems is characterized by particle-particle interactions, modeled as $e^{-i\tau J_z^2}$, where $\tau=\chi(B)T/\hbar$, T is the interrogation time, and $\chi(B)$ is total interaction strength, given by the sum of the elastic particle-particle and the dipolar interaction within each well, see main text. Without loss of generality, we assume that the accumulated phase shift is equal to zero in the following. The quantum state after interrogation stage is thus described by

$$|\psi_{\rm PE}\rangle = \int_{-\infty}^{+\infty} d\mu \; \frac{e^{-\frac{(\mu-\mu_0)^2}{4\sigma^2}}}{(2\pi\sigma^2)^{1/4}} e^{-i\tau\mu^2} \, |\mu\rangle \,, \tag{SI.6}$$

Following Ref. [7], we can evaluate the uncorrelated noise due to intrinsic quantum fluctuations by projecting the state $|\psi_{\rm PE}\rangle$ over phase states

$$|\phi\rangle = \frac{1}{\sqrt{2\pi}} \int_{-\infty}^{+\infty} d\mu \; e^{i\phi\mu} \, |\mu\rangle \,. \tag{SI.7}$$

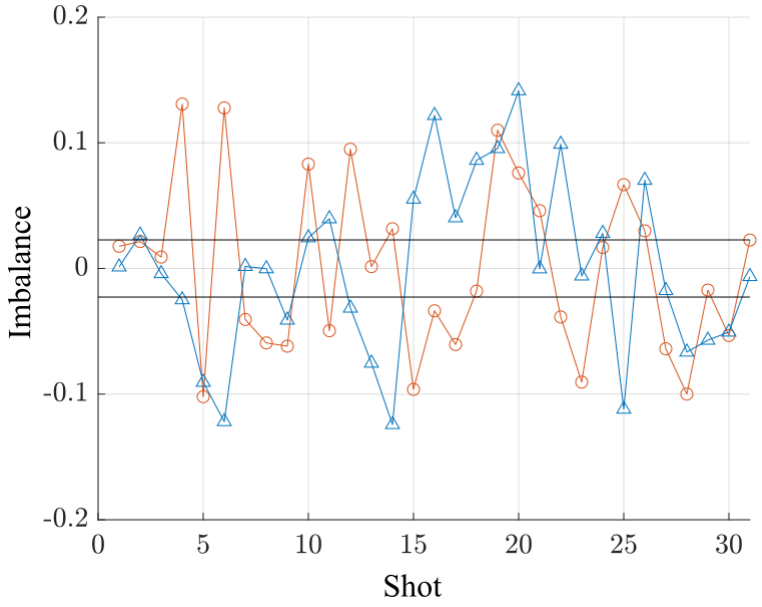

FIGURE 4: **The splitting fluctuation** a) The imbalances z after the splitting sequence as a function of sequence repetition. The blue circle points and the red triangle points are the data of two different double wells that work simultaneously. The black lines represent the value of quantum shots noise for a mean experimental atom number. b) Histogram of the imbalance z for a single DW after the splitting sequence. The blue line is the Gaussian fit of the data and the black line represents the projection noise.

We compute the phase distribution

$$P(\phi|\theta) = |\langle\phi|\,\psi_{\rm PE}\rangle|^2 = \sqrt{\frac{1}{2\pi\sigma^2_{\phi|\theta}}}e^{-\frac{(\phi-\phi_0)^2}{2\sigma^2_{\phi|\theta}}}, \tag{SI.8}$$

obtained from the Fourier transform of the Gaussian function in Eq. (SI.6), where $\phi_0 = N\tau\cos\theta$ and

$$\sigma^2_{\phi|\theta} = \frac{1}{N\sin^2\theta} + N\tau^2\sin^2\theta. \tag{SI.9}$$

In the case $\theta = \pi/2$ we recover the results of Ref. [7]. We now take into account the effect of a noisy beam splitter by considering θ as a (shot-to-shot) stochastic variable with distribution $P(\theta)$. We thus write the phase distribution as

$$P(\phi) = \int_{-\pi}^{\pi} d\theta\; P(\phi|\theta)P(\theta). \tag{SI.10}$$

with

$$P(\theta) = \frac{e^{-\frac{(\theta-\pi/2)^2}{2\sigma^2_{\rm BS}}}}{\sqrt{2\pi\sigma^2_{\rm BS}}}, \tag{SI.11}$$

and $\sigma_{\rm BS}$ quantifying the fluctuations of the beam splitter reflection coefficient θ around the balanced case. Finally, we compute

$$\begin{aligned}\sigma^2_\phi &= \int_{-\infty}^{+\infty} d\phi\; \phi^2 P(\phi)\\ &= \int_{-\infty}^{+\infty} d\theta\; \left(\sigma^2_{\phi|\theta} + \phi_0^2\right)\\ &= \int_{-\infty}^{+\infty} d\theta\; P(\theta)\left[\frac{1}{N\sin^2\theta} + N\tau^2\sin^2\theta\right] + N^2\tau^2\int_{-\infty}^{+\infty} d\theta\; P(\theta)\cos^2\theta.\end{aligned} \tag{SI.12}$$

By expanding the $\sin\theta$ and $\cos\theta$ contribution around $\theta = \pi/2$ and using Eq. (SI.11), we find

$$\sigma_\phi^2 = \frac{1}{N}(1+\sigma_{\rm BS}^2) + N(1-\sigma_{\rm BS}^2)\tau^2 + N^2\tau^2\sigma_{\rm BS}^2. \tag{SI.13}$$

This results provides the intrinsic phase fluctuations for a single interferometer. In the case of two interferometers, the fluctuations are independent and sum up. Assuming for simplicity that the number of particles, noise $\sigma_{\rm BS}$, and interaction strength τ is the same in both interferometers, and considering $N \gg 1$, we have

$$\sigma_{\Delta\phi}^2 = \frac{2}{N}(1+\sigma_{\rm BS}^2) + N\big(1+N\sigma_{\rm BS}^2\big)\,\tau^2. \tag{SI.14}$$

Equation (2) of the main text is recovered taking into account the effect of technical noise and $\tau = \chi(B)T/\hbar$.

We have quantified $\sigma_{\rm BS}$ experimentally. In Fig. 4 we report the values of z recorded after the first beam splitter of the two interferometers (blue triangles and red circles, respectively), as a function of the experimental shots. taking into account that $z = \cos\theta$ and $z \ll 1$, we find that fluctuations of z directly provides the fluctuations of θ, which we have indicated as $\sigma_{\rm BS}$. We find $\sigma_{\rm BS} = 0.0695$ for the red circles and $\sigma_{\rm BS} = 0.069$ and $\sigma_{\rm BS} = 0.068$ for the blue triangles : overall we estimate $\sigma_{\rm BS}^2 = 0.004$, as mentioned in the caption of Fig. 4.

[1] T. Petrucciani, A. Santoni, C. Mazzinghi, D. Trypogeorgos, M. Fattori, and M. Modugno, in preparation (2024).
[2] R. V. Pound, Review of Scientific Instruments **17**, 490 (1946).
[3] R. W. Drever, J. L. Hall, F. V. Kowalski, J. Hough, G. Ford, A. Munley, and H. Ward, Applied Physics B **31**, 97 (1983).
[4] G. Milani, B. Rauf, P. Barbieri, F. Bregolin, M. Pizzocaro, P. Thoumany, F. Levi, and D. Calonico, Opt. Lett. **42**, 1970 (2017), URL `https://opg.optica.org/ol/abstract.cfm?URI=ol-42-10-1970`.
[5] G. Breit and I. I. Rabi, Physical Review **38**, 2082 (1931).
[6] T. Tiecke, University of Amsterdam, The Netherlands, Thesis pp. 12–14 (2010).
[7] J. Javanainen and M. Wilkens, Phys. Rev. Lett. **78**, 4675 (1997).